ARMY RESEARCH LABORATORY

Using Computational Fluid Dynamics-Rigid Body Dynamic (CFD-RBD) Results to Generate Aerodynamic Models for Projectile Flight Simulation

by Mark Costello, Stephen Gatto, and Jubaraj Sahu

ARL-TR-4270 **September 2007**

NOTICES

Disclaimers

The findings in this report are not to be construed as an official Department of the Army position unless so designated by other authorized documents.

Citation of manufacturer's or trade names does not constitute an official endorsement or approval of the use thereof.

DESTRUCTION NOTICE—Destroy this report when it is no longer needed. Do not return it to the originator.

Army Research Laboratory
Aberdeen Proving Ground, MD 21005-5069

ARL-TR-4270 **September 2007**

Using Computational Fluid Dynamics-Rigid Body Dynamic (CFD-RBD) Results to Generate Aerodynamic Models for Projectile Flight Simulation

Mark Costello and Stephen Gatto
Georgia Institute of Technology

Jubaraj Sahu
Weapons and Materials Research Directorate, ARL

REPORT DOCUMENTATION PAGE

Form Approved
OMB No. 0704-0188

1. REPORT DATE *(DD-MM-YYYY)*	2. REPORT TYPE	3. DATES COVERED (From - To)
September 2007	Final	January 2006 to August 2007

4. TITLE AND SUBTITLE

Using Computational Fluid Dynamics-Rigid Body Dynamic (CFD-RBD) Results to Generate Aerodynamic Models for Projectile Flight Simulation

5a. CONTRACT NUMBER

5b. GRANT NUMBER

5c. PROGRAM ELEMENT NUMBER

6. AUTHOR(S)

Mark Costello and Stephen Gatto (GIT); Jubaraj Sahu (ARL)

5d. PROJECT NUMBER
622618AH80

5e. TASK NUMBER

5f. WORK UNIT NUMBER

7. PERFORMING ORGANIZATION NAME(S) AND ADDRESS(ES)
U.S. Army Research Laboratory
Weapons and Materials Research Directorate
Aberdeen Proving Ground, MD 21005-5069

8. PERFORMING ORGANIZATION REPORT NUMBER
ARL-TR-4270

9. SPONSORING/MONITORING AGENCY NAME(S) AND ADDRESS(ES)

10. SPONSOR/MONITOR'S ACRONYM(S)

11. SPONSOR/MONITOR'S REPORT NUMBER(S)

12. DISTRIBUTION/AVAILABILITY STATEMENT

Approved for public release; distribution is unlimited.

13. SUPPLEMENTARY NOTES

14. ABSTRACT

A method to efficiently generate a complete aerodynamic description for projectile flight dynamic modeling is described. At the core of the method is an unsteady, time-accurate computational fluid dynamics simulation that is tightly coupled to a rigid projectile flight dynamic simulation. A set of short time snippets of simulated projectile motion at different Mach numbers is computed and employed as baseline data. For each time snippet, aerodynamic forces and moments and the full rigid body state vector of the projectile are known. With time-synchronized air loads and state vector information, aerodynamic coefficients can be estimated with a simple fitting procedure. By inspecting the condition number of the fitting matrix, we can assess the suitability of the time history data to predict a selected set of aerodynamic coefficients. The technique is exercised on an exemplar fin-stabilized projectile with good results.

15. SUBJECT TERMS
computational fluid dynamics; coupled CFD-RBD; high performance computing; rigid body dynamics

16. SECURITY CLASSIFICATION OF:			17. LIMITATION OF ABSTRACT	18. NUMBER OF PAGES	19a. NAME OF RESPONSIBLE PERSON
a. REPORT	b. ABSTRACT	c. THIS PAGE			Jubaraj Sahu
Unclassified	Unclassified	Unclassified	SAR	35	19b. TELEPHONE NUMBER (*Include area code*) 410-306-0800

Contents

List of Figures

List of Tables

1. Introduction

Four basic methods to predict aerodynamic forces and moments on a projectile in atmospheric flight are commonly used in practice: empirical methods, wind tunnel testing, computational fluid dynamics (CFD) simulation, and spark range testing. Empirical methods have been found very useful in conceptual design of projectiles where rapid and inexpensive estimates of aerodynamic coefficients are needed. These techniques aerodynamically describe the projectile with a set of geometric properties (diameter, number of fins, nose type, nose radius, etc) and catalog aerodynamic coefficients of many different projectiles as a function of these features. These data are fit to multivariable equations to create generic models for aerodynamic coefficients as a function of these basic projectile geometric properties. The database of aerodynamic coefficients as a function of projectile features is typically obtained from wind tunnel or spark range tests. Examples of this approach to projectile aerodynamic coefficient estimation include missile DATCOM, PRODAS, and AP98[1] (*1 through 6*). The advantage of this technique is that it is a general method applicable to any projectile. However, it is the least accurate method of the four methods mentioned, particularly for new configurations that fall outside the realm of projectiles used to form the basic aerodynamic database.

Wind tunnel testing is often used during projectile development programs to converge on fine details of the aerodynamic design of the shell (*7, 8*). In wind tunnel testing, a specific projectile is mounted in a wind tunnel at various angles of attack with aerodynamic forces and moments measured at various Mach numbers via a sting balance. Wind tunnel testing has the obvious advantage of being based on direct measurement of aerodynamic forces and moments on the projectile. It is also relatively easy to change the wind tunnel model to allow detailed parametric effects to be investigated. The main disadvantage of wind tunnel testing is that it requires a wind tunnel and is therefore modestly expensive. Furthermore, dynamic derivatives such as pitch and roll damping as well as Magnus force and moment coefficients are difficult to obtain in a wind tunnel and require a complex physical wind tunnel model.

Over the past couple of decades, tremendous strides have been made in the application of CFD to predict aerodynamic loads on air vehicles including projectiles. These methods are increasingly being used throughout the weapon development cycle including early in a program to create relatively low cost estimates of aerodynamic characteristics and later in a program to supplement and reduce expensive experimental testing. In CFD simulation, the fundamental fluid dynamic equations are numerically solved for a specific configuration. The most sophisticated computer codes are capable of unsteady time-accurate computations with the use of Navier-Stokes equations. Examples of these tools include, for example, CFD++, Fluent, and Overflow-D. CFD is computationally expensive, requires powerful computers to obtain results in a reasonably timely manner,

[1]DATCOM is not an acronym; PRODAS = Projectile Design and Analysis System; AP98 = AeroPrediction98.

and requires dedicated engineering specialists to drive these tools (*9 through 24*). Spark range aerodynamic testing has long been considered the gold standard for projectile aerodynamic coefficient estimation. It is the most accurate method for obtaining aerodynamic data on a specific projectile configuration. In spark range aerodynamic testing, a projectile is fired through an enclosed building. At a discrete number of points during the flight of the projectile (< 30), the state of the projectile is measured via spark shadowgraphs (*25 through 29*). The projectile state data are subsequently fit to a rigid six-degree-of-freedom (6-DOF) projectile model with the use of the aerodynamic coefficients as the fitting parameters (*30, 31, 32*). Although this technique is the most accurate method for obtaining aerodynamic data on a specific projectile configuration, it is usually the most expensive alternative, requires a spark range facility, and (strictly speaking) is only valid for the specific projectile configuration tested.

Various researchers have used CFD to estimate aerodynamic coefficient estimation of projectiles. Early work focused on Euler solvers applied to steady flow problems, while more recent work has solved the Reynolds-averaged Navier-Stokes equations and large eddy simulation Navier-Stokes equations for steady and unsteady conditions (*9 through 24*). For example, to predict pitch damping, Weinacht prescribed projectile motion to mimic a typical pitch-damping wind tunnel test in a CFD simulation to estimate the different components of the pitch-damping coefficient of a fin-stabilized projectile (*33*). Excellent agreement between computed and measured pitch damping was attained. Algorithm and computing advances have also led to the coupling of CFD codes to projectile rigid body dynamics (RBD) codes to simulate free flight motion of a projectile in a time-accurate manner. Aerodynamic forces and moments are computed with the CFD solver while the free flight motion of the projectile is computed by the integration of the RBD equations of motion. Sahu achieved excellent agreement between spark range measurements and a coupled CFD-RBD approach for a fin-stabilized projectile (*34*). Projectile position and orientation at down-range locations consistent with a spark range test were extracted from the output of the CFD-RBD software to compute aerodynamic coefficients. Standard range reduction software was used for this purpose with good agreement obtained when contrasted against sample spark range results. The ability to accurately compute projectile aerodynamics in highly unsteady conditions has led to the notion of “virtual wind tunnels” and “virtual fly-outs” where the simulation tools are used to replicate a wind tunnel or spark range test.

Computation time for accurate coupled CFD-RBD simulation remains exceedingly high and does not currently represent a practical method for typical flight dynamic analysis such as impact point statistics (e.g., circular error probable) computation where thousands of “fly-outs” are required. Furthermore, this type of analysis does not allow the same level of understanding of the inherent underlying dynamics of the system that RBD analysis with aerodynamic coefficients yields. However, the coupled CFD-RBD approach does offer an indirect way to rapidly compute the aerodynamic coefficients needed for rigid 6-DOF simulation. During a time-accurate CFD-RBD simulation, aerodynamic forces and moments and the full rigid body state vector of the projectile are generated at each time step in the simulation (*34*). This means that aerodynamic forces,

aerodynamic moments, position of the mass center, body orientation, translational velocity, and angular velocity of the projectile are all known at the same time instant. With time-synchronized air load and state vector information, the aero-dynamic coefficients can be estimated with a simple fitting procedure. This report creates a method to efficiently generate a complete aerodynamic model for a projectile in atmospheric flight with four short time histories at each Mach number of interest with an industry standard time-accurate CFD-RBD simulation. The technique is exercised on sample CFD-RBD data for a small fin-stabilized projectile. Parametric trade studies investigating the required length of each time snippet as well as the required CFD accuracy are reported.

2. Projectile CFD-RBD Simulation

The projectile CFD-RBD algorithm employed here combines a rigid 6-DOF projectile flight dynamic model with a three-dimensional (3-D), time-accurate CFD simulation. The RBD dynamic equations are integrated forward in time where aerodynamic forces and moments that drive the motion of the projectile are computed via the CFD algorithm. The RBD projectile model allows for three translational degrees of freedom and three rotational degrees of freedom. As shown in figures 1 and 2, the I frame is attached to the ground while the B frame is fixed to the projectile with the $\vec{I}_B$ axis pointing out the nose of the projectile and the $\vec{J}_B$ and $\vec{K}_B$ unit vectors forming a right-handed triad. The projectile state vector is comprised of the inertial position components of the projectile mass center (x, y, z), the standard aerospace sequence Euler angles (ϕ, θ, ψ), the body frame components of the projectile mass center velocity (u, v, w), and the body frame components of the projectile angular velocity vector (p, q, r).

Both the translational and rotational dynamic equations are expressed in the projectile body reference frame. The standard rigid projectile, body frame equations of motion are given by equations 1 through 4.

$$\begin{Bmatrix} \dot{x} \\ \dot{y} \\ \dot{z} \end{Bmatrix} = \begin{bmatrix} c_\theta c_\psi & s_\phi s_\theta c_\psi - c_\phi s_\psi & c_\phi s_\theta c_\psi + s_\phi s_\psi \\ c_\theta s_\psi & s_\phi s_\theta s_\psi + c_\phi c_\psi & c_\phi s_\theta s_\psi - s_\phi c_\psi \\ -s_\theta & s_\phi c_\theta & c_\phi c_\theta \end{bmatrix} \begin{Bmatrix} u \\ v \\ w \end{Bmatrix} \tag{1}$$

$$\begin{Bmatrix} \dot{\phi} \\ \dot{\theta} \\ \dot{\psi} \end{Bmatrix} = \begin{bmatrix} 1 & s_\phi t_\theta & c_\phi t_\theta \\ 0 & c_\phi & -s_\phi \\ 0 & s_\phi / c_\theta & c_\phi / c_\theta \end{bmatrix} \begin{Bmatrix} p \\ q \\ r \end{Bmatrix} \tag{2}$$

$$\begin{Bmatrix} \dot{u} \\ \dot{v} \\ \dot{w} \end{Bmatrix} = \begin{Bmatrix} X/m \\ Y/m \\ Z/m \end{Bmatrix} - \begin{bmatrix} 0 & -r & q \\ r & 0 & -p \\ -q & p & 0 \end{bmatrix} \begin{Bmatrix} u \\ v \\ w \end{Bmatrix} \tag{3}$$

$$\begin{Bmatrix} \dot{p} \\ \dot{q} \\ \dot{r} \end{Bmatrix} = [I]^{-1} \left[\begin{Bmatrix} L \\ M \\ N \end{Bmatrix} - \begin{bmatrix} 0 & -r & q \\ r & 0 & -p \\ -q & p & 0 \end{bmatrix} [I] \begin{Bmatrix} p \\ q \\ r \end{Bmatrix} \right] \tag{4}$$

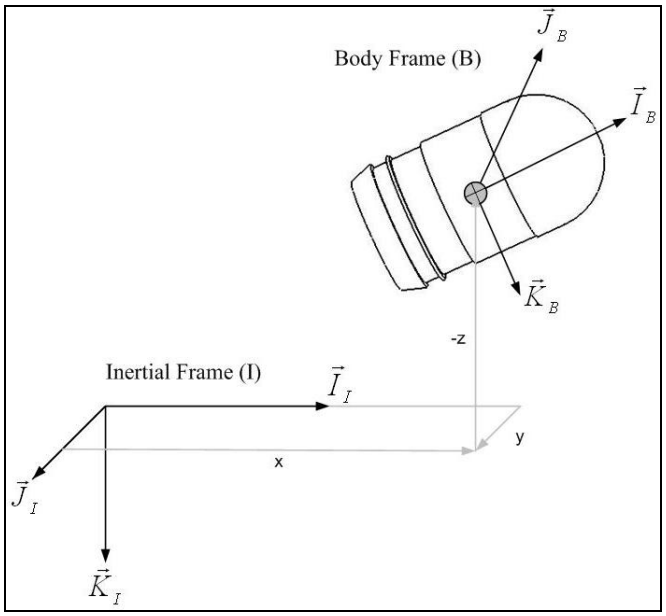

Figure 1. Reference frame and position definitions.

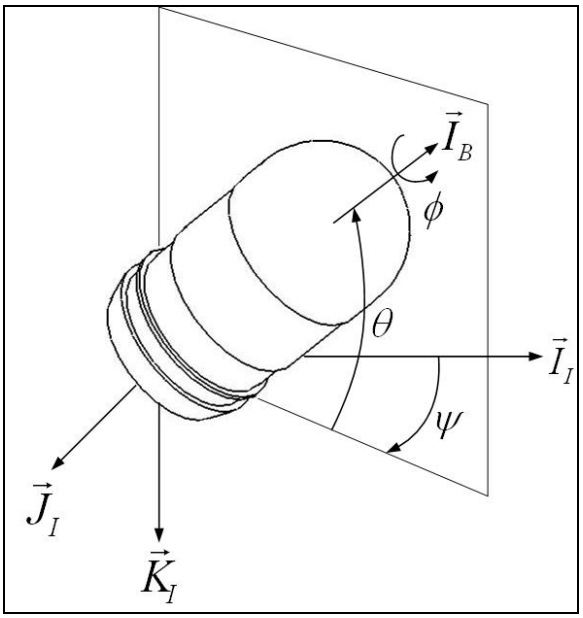

Figure 2. Projectile orientation definitions.

Note that the total applied force components (X, Y, Z) and moment components (L, M, N) contain contributions from weight and aerodynamics. The aerodynamic portion of the applied loads in equations 3 and 4 is computed with the CFD simulation and passed to the RBD simulation.

On the other hand, the CFD flow equations are integrated forward in time where the motion of the projectile that drives flow dynamics are computed with the RBD algorithm. The complete set of 3-D time-dependent Navier-Stokes equations is solved in a time-accurate manner for simulation of free flight. The commercially available code, CFD++, is used for the time-accurate unsteady CFD simulations (*35, 36*). The basic numerical framework in the code contains unified grid, unified physics, and unified computing features. The 3-D, time-dependent Reynolds-averaged Navier-Stokes (RANS) equations are solved with the following finite volume equation.

$$\frac{\partial}{\partial t}\int_V W dV + \oint (F - G)\, dA = \int_V H dV \tag{5}$$

in which **W** is the vector of conservative variables, **F** and **G** are the inviscid and viscous flux vectors, respectively, **H** is the vector of source terms, **V** is the cell volume, and **A** is the surface area of the cell face. A second order discretization is used for the flow variables and the turbulent viscosity equation. The turbulence closure is based on topology-parameter-free formulations. Two-equation higher order RANS turbulence models are used for the computation of turbulent flows. These models are ideally suited to unstructured bookkeeping and massively parallel processing because of their independence from constraints related to the placement of boundaries and/or zonal interfaces.

A dual time-stepping approach is used to integrate the flow equations to achieve the desired time accuracy. The first is an "outer" or global (and physical) time step that corresponds to the time discretization of the physical time variation term. This time step can be chosen directly by the user and is typically set to a value to represent 1/100 of the period of oscillation expected or forced in the transient flow. It is also applied to every cell and is not spatially varying. An artificial or "inner" or "local" time variation term is added to the basic physical equations. This time step and corresponding "inner iteration" strategy is chosen to help satisfy the physical transient equations to the desired degree. For the inner iterations, the time step is allowed to vary spatially. Also, relaxation with multi-grid (algebraic) acceleration is employed to reduce the residues of the physical transient equations. It is found that an order of magnitude reduction in the residues is usually sufficient to produce a good transient iteration.

The projectile in the coupled CFD-RBD simulation, along with its grid, moves and rotates as the projectile flies down range. Grid velocity is assigned to each mesh point. For a spinning and yawing projectile, the grid speeds are assigned as if the grid were attached to the projectile and spinning and yawing with it.

In order to properly initialize the CFD simulation, two modes of operation for the CFD code are used, namely, an uncoupled and a coupled mode. The uncoupled mode is used to initialize the CFD flow solution while the coupled mode represents the final time accurate coupled CFD-RBD solution. In the uncoupled mode, the RBD are specified. The uncoupled mode begins with a computation performed in "steady state mode" with the grid velocities prescribed to account for the proper initial position (x_0, y_0, z_0), orientation (ϕ_0, θ_0, ψ_0), and translational velocity (u_0, v_0, w_0) components of the complete set of initial conditions to be prescribed. After the steady state solution is converged, the initial spin rate (p_0) is included and a new quasi-steady state solution is obtained with time-accurate CFD. A sufficient number of time steps are performed so that the angular orientation for the spin axis corresponds to the prescribed initial conditions. This quasi-steady state flow solution is the starting point for the time-accurate coupled solution. For the coupled solution, the mesh is translated back to the desired initial position (x_0, y_0, z_0) and the remaining angular velocity initial conditions (q_0, r_0) are then added. In the coupled mode, the aerodynamic forces and moments are passed to the RBD simulation which propagates the rigid state of the projectile forward in time.

3. Flight Dynamic Projectile Aerodynamic Model

The applied loads in equations 3 and 4 contain contributions from projectile weight and body aerodynamic forces and moments:

$$\begin{Bmatrix} X \\ Y \\ Z \end{Bmatrix} = W \begin{Bmatrix} -s_\theta \\ s_\phi c_\theta \\ c_\phi c_\theta \end{Bmatrix} - \frac{\pi}{8} \rho V^2 D^2 \begin{Bmatrix} C_{X0} + C_{X2}(v^2 + w^2)/V^2 \\ C_{NA} v/V - \dfrac{pD}{2V} C_{YPA} w/V \\ C_{NA} w/V + \dfrac{pD}{2V} C_{YPA} v/V \end{Bmatrix} \tag{6}$$

$$\begin{Bmatrix} L \\ M \\ N \end{Bmatrix} = \frac{\pi}{8} \rho V^2 D^3 \begin{Bmatrix} C_{LDD} + \dfrac{pD}{2V} C_{LP} \\ C_{MA} \dfrac{w}{V} + \dfrac{qD}{2V} C_{MQ} + \dfrac{pD}{2V} C_{NPA} \dfrac{v}{V} \\ -C_{MA} \dfrac{v}{V} + \dfrac{rD}{2V} C_{MQ} + \dfrac{pD}{2V} C_{NPA} \dfrac{w}{V} \end{Bmatrix} \tag{7}$$

The terms containing C_{YPA} constitute the Magnus air load acting at the Magnus center of pressure while the terms containing C_{X0}, C_{X2}, C_{NA} define the steady load acting at the center of pressure. The externally applied moment about the projectile mass center is composed of an unsteady aerodynamic moment along with terms because the center of pressure and center of Magnus are

not located at the mass center. The terms involving C_{MA} account for the center of pressure being located off the mass center while the terms involving C_{NPA} account for the center of Magnus being located off the mass center. The aerodynamic coefficients are all a function of local Mach number which are typically handled through a table look-up scheme in projectile flight simulation codes.

4. Projectile Aerodynamic Coefficient Estimation (PACE)

The time-accurate coupled CFD-RBD simulation provides a full flow solution, including the aerodynamic portion of the total applied force and moment (X, Y, Z, L, M, N) along with the full state of the rigid projectile ($x, y, z, \phi, \theta, \psi, u, v, w, p, q, r$) at every time step in the solution for each time snippet. Given a set of n short time histories (snippets) that each contain m time points, we obtain a total of $h = m*n$ time history data points for use in estimating the aerodynamic coefficients: $C_{X0}, C_{X2}, C_{NA}, C_{YPA}, C_{LDD}, C_{LP}, C_{MA}, C_{MQ}, C_{NPA}$. Note that for fin-stabilized projectile configurations, the Magnus force and moment are usually sufficiently small so that C_{YPA} and C_{NPA} are set to zero and removed from the fitting procedure to be described next.

Equations 6 and 7 represent the applied air loads on the projectile expressed in the projectile body frame. Computation of the aerodynamic coefficients is aided by transformation of these equations to the instantaneous aerodynamic angle of attack reference frame that rotates the projectile body frame about the $\vec{I}_B$ axis by the angle $\gamma = \tan^{-1}(w/v)$.

$$-\frac{8}{\pi\rho V^2 D^2}\begin{bmatrix}1 & 0 & 0\\ 0 & c_\gamma & s_\gamma\\ 0 & -s_\gamma & c_\gamma\end{bmatrix}\left(\begin{Bmatrix}X\\ Y\\ Z\end{Bmatrix} - W\begin{Bmatrix}-s_\theta\\ s_\phi c_\theta\\ c_\phi c_\theta\end{Bmatrix}\right) = \begin{Bmatrix}C_{X0} + C_{X2}(v^2+w^2)/V^2\\ C_{NA}\dfrac{\sqrt{v^2+w^2}}{V}\\ \dfrac{pD}{2V}\dfrac{\sqrt{v^2+w^2}}{V}C_{YPA}\end{Bmatrix} \tag{8}$$

$$\frac{8}{\pi\rho V^2 D^3}\begin{bmatrix}1 & 0 & 0\\ 0 & c_\gamma & s_\gamma\\ 0 & -s_\gamma & c_\gamma\end{bmatrix}\begin{Bmatrix}L\\ M\\ N\end{Bmatrix} = \begin{Bmatrix}C_{LDD} + \dfrac{pD}{2V}C_{LP}\\ \dfrac{(vq+wr)D}{2\sqrt{v^2+w^2}V}C_{MQ} + \dfrac{pD}{2V}\dfrac{\sqrt{v^2+w^2}}{V}C_{NPA}\\ \dfrac{(vr-wq)D}{2\sqrt{v^2+w^2}V}C_{MQ} - \dfrac{\sqrt{v^2+w^2}}{V}C_{MA}\end{Bmatrix} \tag{9}$$

Each time history data point provides a total of six equations given by the components of equations 8 and 9. The first component of equation 8 is gathered together for all time history data points to

form equation 10. Likewise, the second and third components of equation 8 generate equations 11 and 12, respectively, while the first component of equation 9 constructs equation 13. Finally, the second and third components of equation 9 are gathered together to form equation 14. Subscripts on the projectile state vector and aerodynamics force and moment components represent the time history data point.

$$\begin{bmatrix} 1 & (v_1^2+w_1^2)/V_1^2 \\ \vdots & \vdots \\ 1 & (v_h^2+w_h^2)/V_h^2 \end{bmatrix} \begin{Bmatrix} C_{X0} \\ C_{X2} \end{Bmatrix} = \begin{Bmatrix} -\dfrac{8}{\pi\rho V_1^2 D^2}\left(X_1 + W\sin\theta_1\right) \\ \vdots \\ -\dfrac{8}{\pi\rho V_h^2 D^2}\left(X_h + W\sin\theta_h\right) \end{Bmatrix} \tag{10}$$

$$\begin{bmatrix} \sqrt{v_1^2+w_1^2}/V_1 \\ \vdots \\ \sqrt{v_h^2+w_h^2}/V_h \end{bmatrix} \{C_{NA}\} = \begin{Bmatrix} -\dfrac{8}{\pi\rho V_1^2 D^2}\left(Y_1\cos\gamma_1 + Z_1\sin\gamma_1 - W\sin\phi_1\cos\theta_1\right) \\ \vdots \\ -\dfrac{8}{\pi\rho V_h^2 D^2}\left(Y_h\cos\gamma_h + Z_h\sin\gamma_h - W\sin\phi_h\cos\theta_h\right) \end{Bmatrix} \tag{11}$$

$$\begin{bmatrix} \dfrac{p_1 D\sqrt{v_1^2+w_1^2}}{2V_1^2} \\ \vdots \\ \dfrac{p_h D\sqrt{v_h^2+w_h^2}}{2V_h^2} \end{bmatrix} \{C_{YPA}\} = \begin{Bmatrix} -\dfrac{8}{\pi\rho V_1^2 D^2}\left(-Y_1\sin\gamma_1 + Z_1\cos\gamma_1 - W\cos\phi_1\cos\theta_1\right) \\ \vdots \\ -\dfrac{8}{\pi\rho V_h^2 D^2}\left(-Y_h\sin\gamma_h + Z_h\cos\gamma_h - W\cos\phi_h\cos\theta_h\right) \end{Bmatrix} \tag{12}$$

$$\begin{bmatrix} 1 & \dfrac{p_1 D}{2V_1} \\ \vdots & \vdots \\ 1 & \dfrac{p_h D}{2V_h} \end{bmatrix} \begin{Bmatrix} C_{LDD} \\ C_{LP} \end{Bmatrix} = \begin{Bmatrix} \dfrac{8L_1}{\pi\rho V_1^2 D^3} \\ \vdots \\ \dfrac{8L_h}{\pi\rho V_h^2 D^3} \end{Bmatrix} \tag{13}$$

$$\begin{bmatrix} 0 & \dfrac{(v_1 q_1 + w_1 r_1)D}{2V_1\sqrt{v_1^2 + w_1^2}} & \dfrac{p_1 D\sqrt{v_1^2 + w_1^2}}{2V_1^2} \\ -\dfrac{\sqrt{v_1^2 + w_1^2}}{V_1} & \dfrac{(v_1 r_1 - w_1 q_1)D}{2V_1\sqrt{v_1^2 + w_1^2}} & 0 \\ \vdots & \vdots & \vdots \\ 0 & \dfrac{(v_h q_h + w_h r_h)D}{2V_h\sqrt{v_h^2 + w_h^2}} & \dfrac{p_h D\sqrt{v_h^2 + w_h^2}}{2V_h^2} \\ -\dfrac{\sqrt{v_h^2 + w_h^2}}{V_h} & \dfrac{(v_h r_h - w_h q_h)D}{2V_h\sqrt{v_h^2 + w_h^2}} & 0 \end{bmatrix} \begin{Bmatrix} C_{MA} \\ C_{MQ} \\ C_{NPA} \end{Bmatrix} = \begin{Bmatrix} \dfrac{8}{\pi\rho V_1^2 D^3}\left(M_1 \cos\gamma_1 + N_1 \sin\gamma_1\right) \\ \dfrac{8}{\pi\rho V_1^2 D^3}\left(-M_1 \sin\gamma_1 + N_1 \cos\gamma_1\right) \\ \vdots \\ \dfrac{8}{\pi\rho V_h^2 D^3}\left(M_h \cos\gamma_h + N_h \sin\gamma_h\right) \\ \dfrac{8}{\pi\rho V_h^2 D^3}\left(-M_h \sin\gamma_h + N_h \cos\gamma_h\right) \end{Bmatrix} \quad (14)$$

Equations 10 through 14 represent a set of five uncoupled problems to solve for the different aerodynamic coefficients. To estimate the aerodynamic coefficients near a particular Mach number, a set of n time accurate coupled CFD-RBD simulations are created over a relatively short time period. Since an individual time snippet is over a short time period where the projectile state variables does not change appreciably, it is critical that initial conditions for the different time snippet be selected in an informed way so that the rank of each of the fitting matrices is maximal. Properties of the fitting matrices, such as the rank or condition number, can be used as an indicator of the suitability of the CFD-RBD simulation data to estimate the aerodynamic coefficients at the target Mach number. Equation 10 is employed to estimate the zero yaw drag coefficient (C_{X0}) and the yaw drag coefficient (C_{X2}). To minimize the condition number of this fitting matrix, both low and high aerodynamic angle of attack time snippets are required. Equation 11 is used to compute the normal force coefficient (C_{NA}) and it requires time history data with a non-zero aerodynamic angle of attack. Equation 12 is used to compute the Magnus force coefficient (C_{YPA}) and it requires time history data with both low and high roll rate and aerodynamic angle of attack. Equation 13 is employed to estimate the fin cant roll coefficient (C_{LDD}) along with the roll-damping coefficient (C_{LP}). To minimize the condition number of this fitting matrix, both low and high roll rate time snippets are required. Equation 14 is employed to estimate the pitching moment coefficient (C_{MA}), the pitch-damping coefficient (C_{MQ}), and the Magnus moment coefficient (C_{NPA}). For successful estimation of these coefficients, time history data with both low and high roll rate and aerodynamic angle of attack as well as low and high aerodynamic angle of attack are required. To meet all the requirements for successful estimation of all five sets of aerodynamic coefficients, four time snippets are used, all with different initial conditions. Table 1 lists the four cases with launch conditions. Notice that the set of time snippets contains a diverse set of initial conditions: zero aerodynamic angle of attack and angular rates; high angle of attack and zero angular rates; low angle of attack, high roll rate with other angular rates zero; zero angle of attack, high pitch rate with other angular rates zero.

Table 1. Time snippet initial conditions.

State	Case 1	Case 2	Case 3	Case 4
x (m)	0	0	0	0
y (m)	0	0	0	0
z (m)	0	0	0	0
Phi (deg)	0	0	0	0
Theta (deg)	0	0	0	0
Psi (deg)	0	0	0	0
V(m/s)	1032	1032	1032	1032
v (m/s)	0	0	0	0
w (m/s	0	-352.5	-90	0
p (rad/s)	0	0	377	0
q (rad/s)	0	0	0	-10
r (rad/s)	0	0	0	0
Alpha (deg)	0	20	5	0

For flight dynamic simulation, aerodynamic coefficients are required at a set of Mach numbers that covers the intended spectrum of flight conditions for the round. If aerodynamic coefficients are estimated at k different Mach numbers, then a total of $l = k * n$ time snippets must be generated to construct the entire aerodynamic database for flight simulation purposes.

5. Results

In order to exercise the method developed, a generic finned projectile is considered. A sketch of the projectile is shown in figure 3. The projectile has the following geometric and mass properties: length = 0.1259 m, reference diameter = 0.013194 m, mass = 0.0484 kg, mass center location from base = 0.0686 m, roll inertia = 0.74E-06 kg m^2, pitch inertia = 0.484E-04 kg m^2.

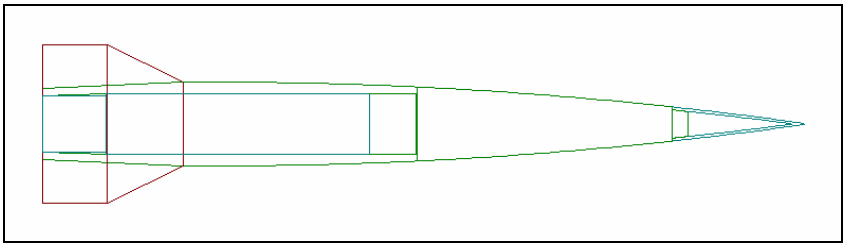

Figure 3. Unstructured mesh near the finned body.

Figures 4 through 9 present projectile state trajectories for each of the four time snippets. Each time snippet is 0.023 second and contains 50 points, leading to an average output time step of 0.0004. The initial conditions for each of the time snippets are shown in table 1. These four snippets create time history data at low and high angle of attack, roll rate, and pitch rate needed for accurate aerodynamic coefficient estimation. Notice that Cases 2 and 3 have notably more drag because of the high angle of attack launch conditions. Case 3 is launched with relatively high roll

rate compared to all other cases. Case 4 generates roll rate toward the end of the time snippet because of high angle of attack roll-pitch coupling. Significant oscillations in Euler pitch angle are created in Case 2 with some cross-coupling response exhibited in Euler yaw angle. Figures 10 through 15 plot aerodynamic forces and moments in the local angle of attack reference frame defined for Cases 1, 3, and 4 since these cases are the primary ones used to estimate the coefficients. For all cases, the axial force oscillates from -20 N to -25 N. There exists a slight bias between the CFD-RBD and estimated data of about 0.5 N for low angle of attack time snippets. For moderately high angles of attack (Case 3), the estimated data also oscillate with a much higher amplitude than the CFD-RBD data, indicating that CX2 is estimated larger than the CFD-RBD suggests. The normal force time snippets agree well between the CFD-RBD and estimated data for all time snippets. For the sample finned projectile, side force and out-of-plane moment are generally small (< 0.5 N, 0.05 Newton meters [Nm]) because of a negligibly small Magnus force and moment. The CFD-RBD and estimated data agree reasonably well but certainly do not overlie one another. The only time snippet that creates notable rolling moment is Case 3 which is launched with an initial roll rate of 377 rad/sec. Notice that the estimated data smoothly go through the CFD-RBD data which oscillate in a slightly erratic manner. The in-plane moment (Mz) agrees reasonably well for both the CFD-RBD and estimated data. The results shown in figures 4 through 15 are typical for all Mach numbers. The overall observation from the data is that the estimated aerodynamic model fits the CFD-RBD data well, with the notable exception of axial force where a bias between the two is exhibited.

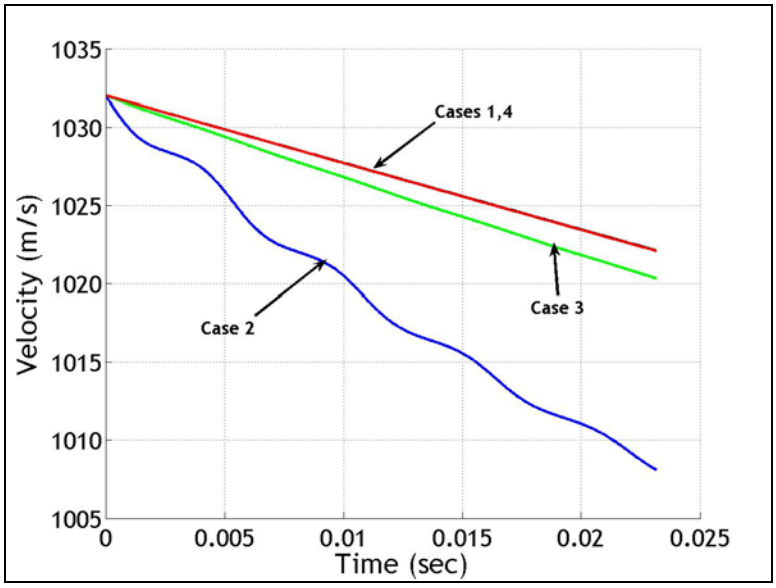

Figure 4. Velocity for the time snippets.

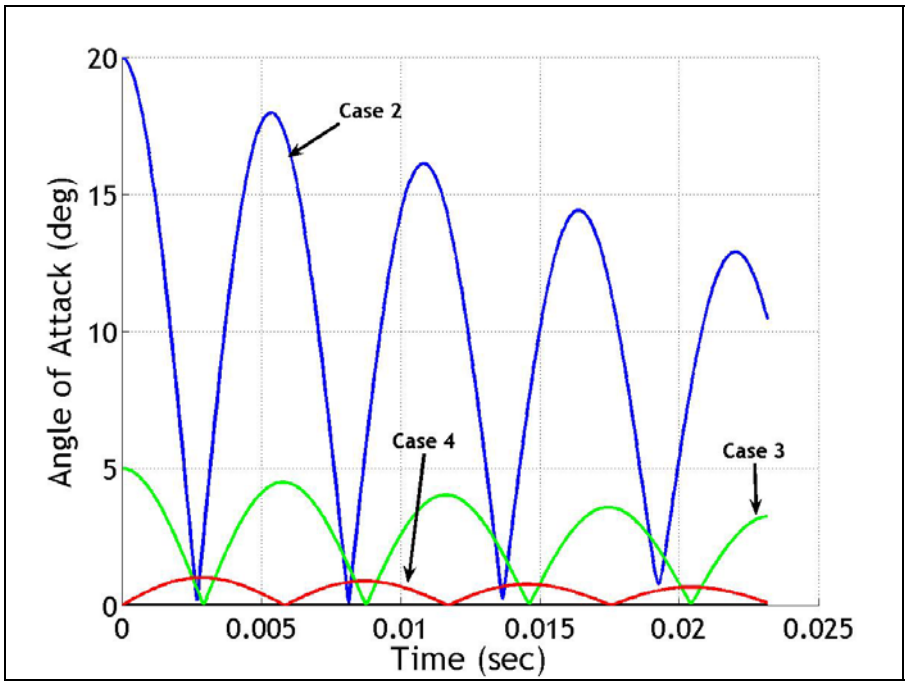

Figure 5. Aerodynamic angle of attack for the time snippets.

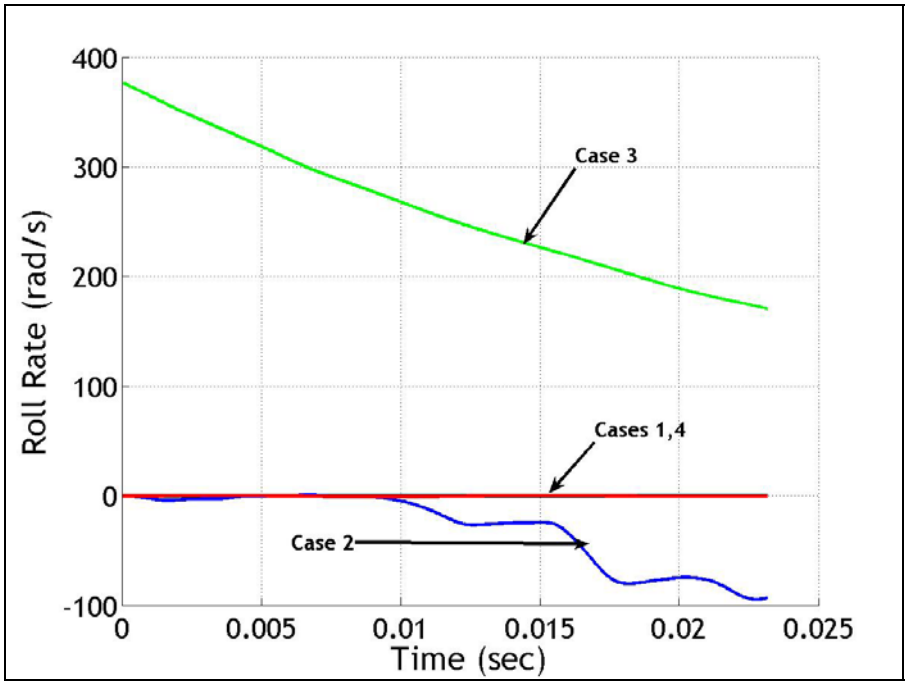

Figure 6. Roll rate for the time snippets.

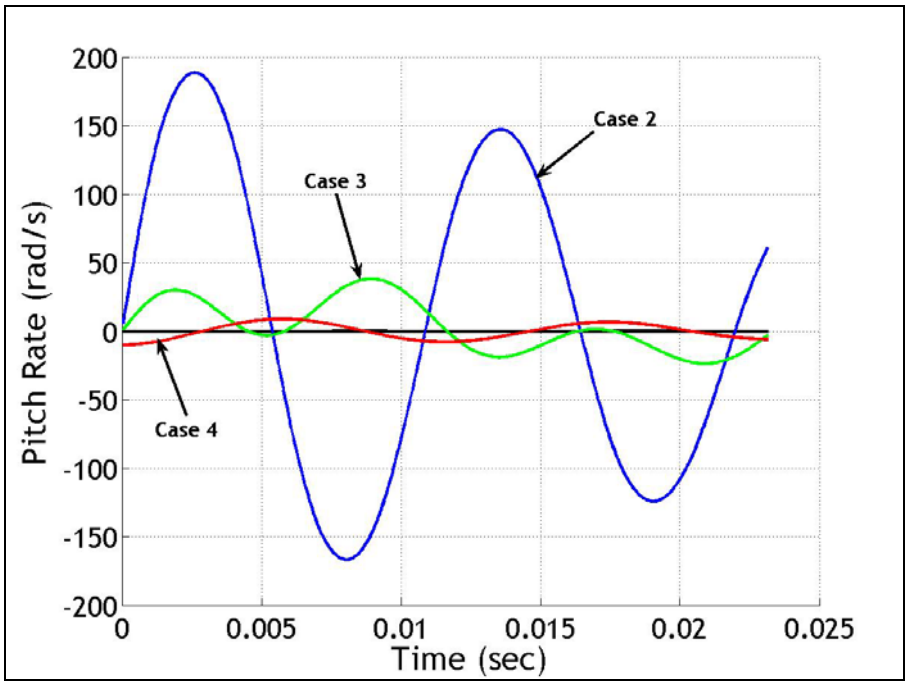

Figure 7. Pitch rate for the time snippets.

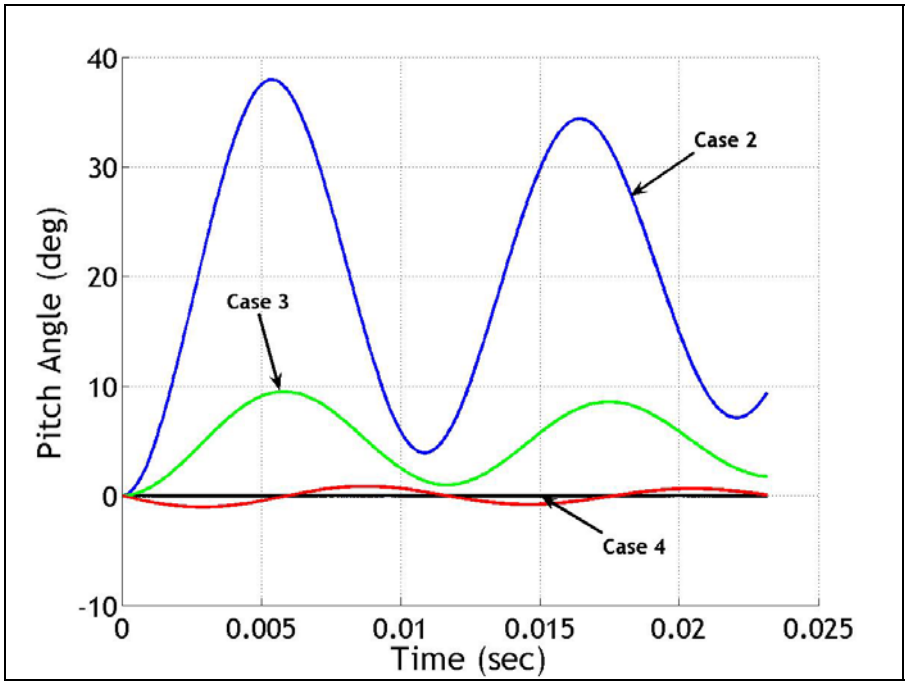

Figure 8. Euler pitch angle for the time snippets.

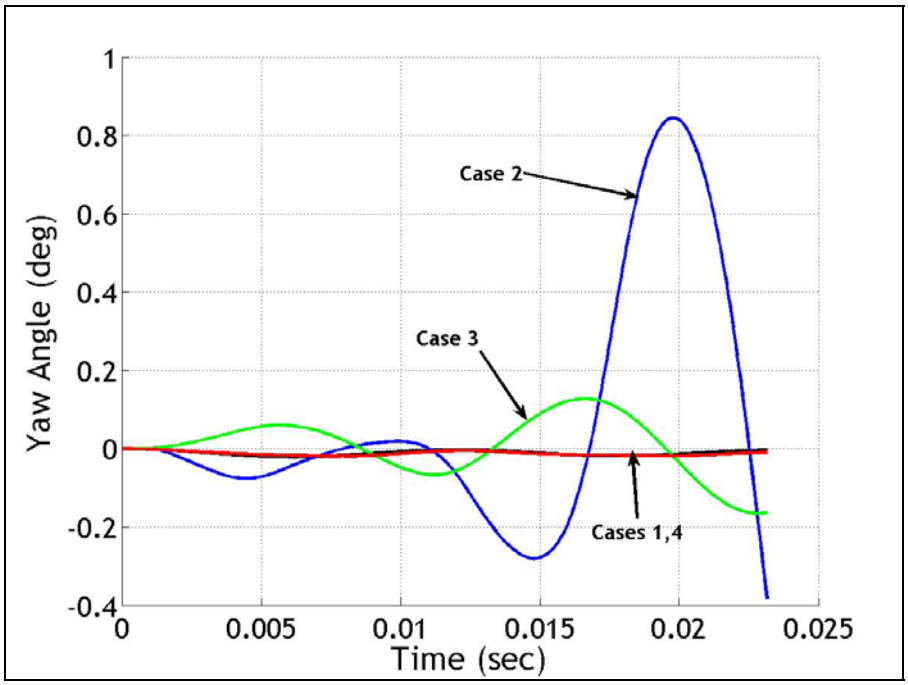

Figure 9. Euler yaw angle for the time snippets.

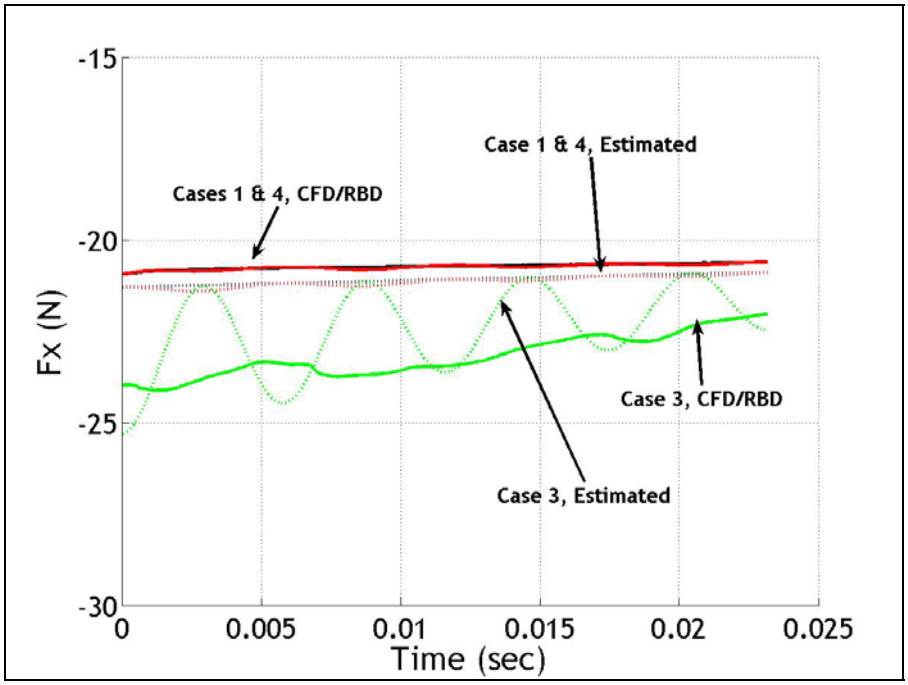

Figure 10. Estimated (dashed) and CFD-RBD (solid) body axis axial force (Fx) versus time.

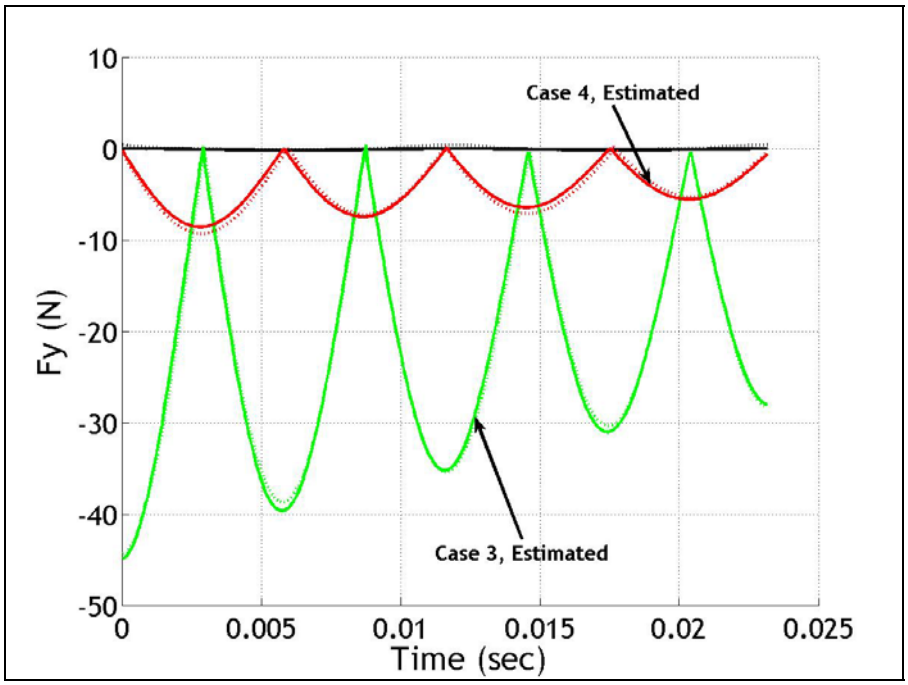

Figure 11. Estimated (dashed) and CFD-RBD (solid) normal force (Fy) versus time.

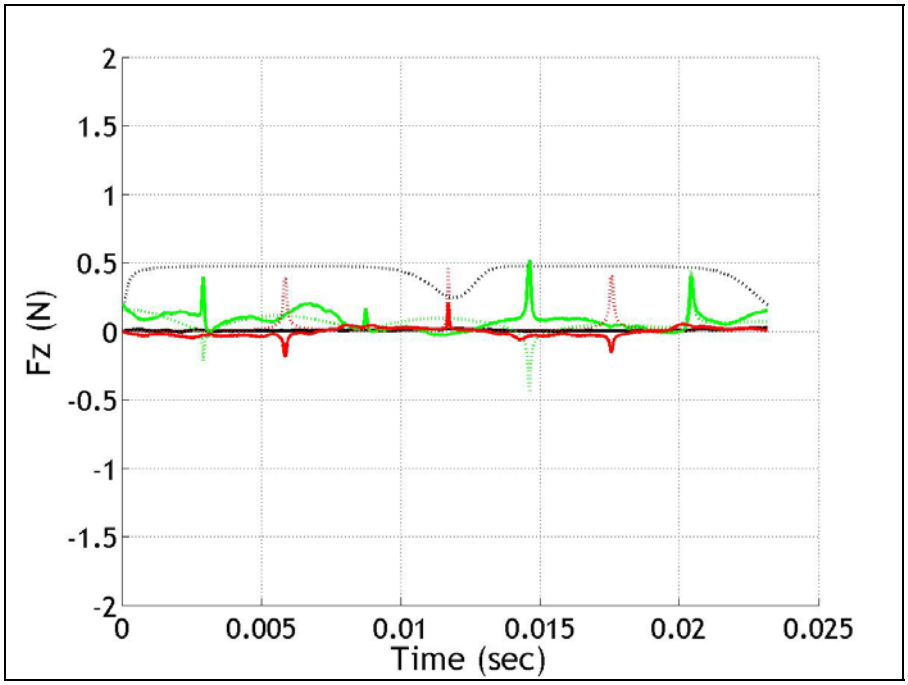

Figure 12. Estimated (dashed) and CFD-RBD (solid) side force (Fz) versus time.

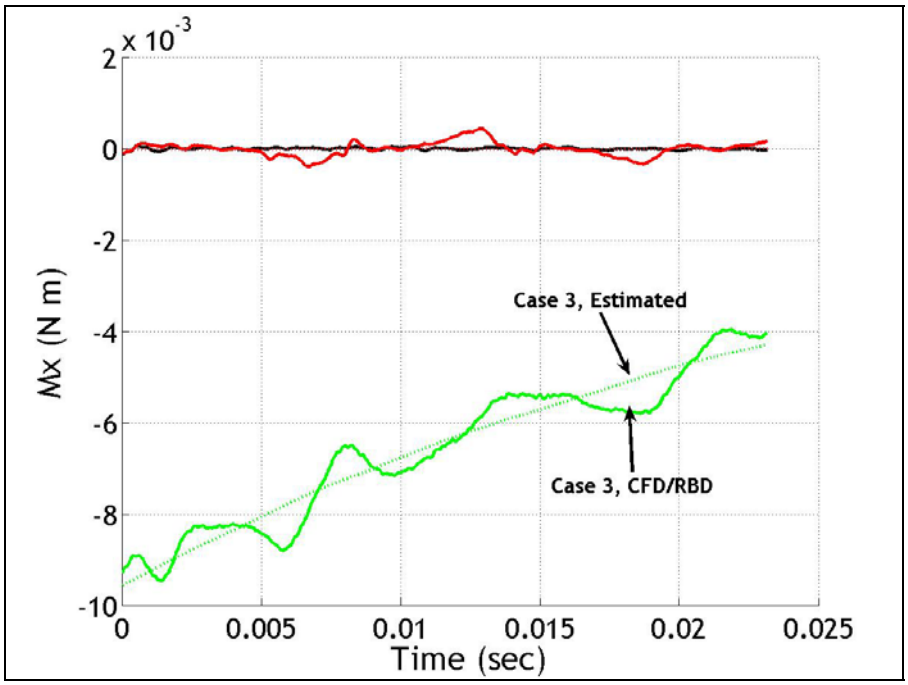

Figure 13. Estimated (dashed) and CFD-RBD (solid) body axis rolling moment (Mx) versus time.

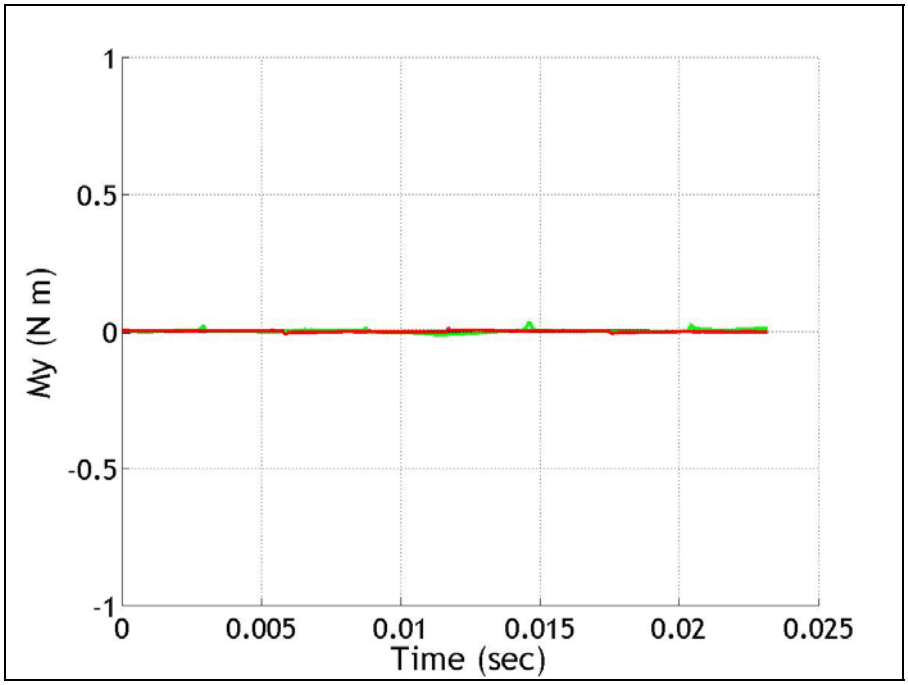

Figure 14. Estimated (dashed) and CFD-RBD (solid) pitching moment (My) versus time.

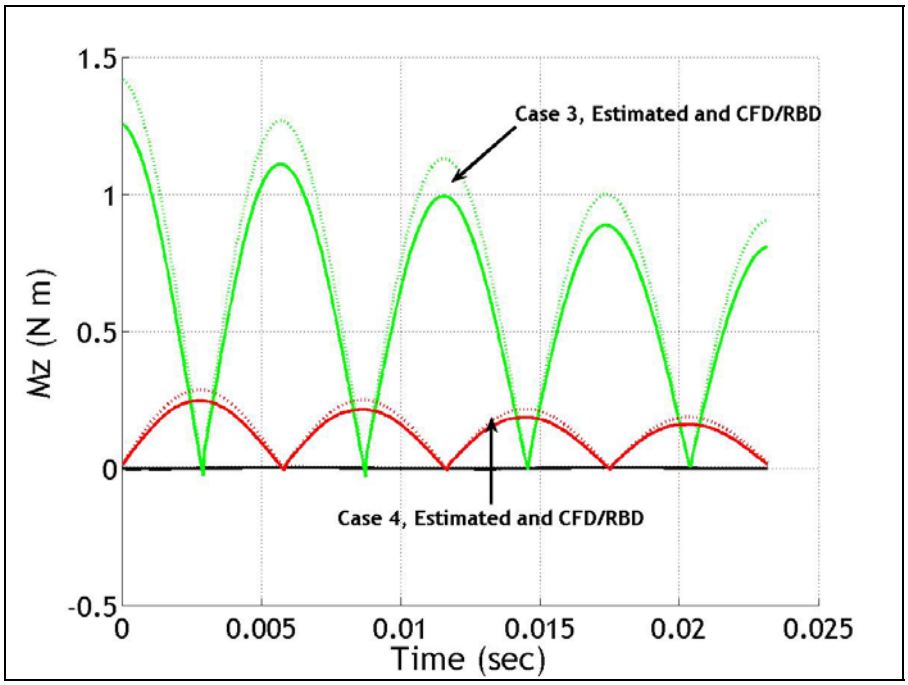

Figure 15. Estimated (dashed) and CFD-RBD (solid) yawing moment (Mz) versus time.

The sample projectile investigated in this report has been fired in a spark range at Mach 3.0 with aerodynamic coefficients computed via conventional aerodynamic range reduction. Table 2 presents a comparison of aerodynamic coefficients obtained from spark range testing and subsequent coefficients obtained with the method described here. Notice that most aerodynamic coefficients such as C_{X0}, C_{NA}, and C_{MA} are in reasonably good agreement with the test data. Axial force yaw drag and roll damping are both different by ~20%, while pitch damping is different by ~40%. Differences in the spark range and estimated coefficients can be attributed to several factors, such as inaccuracies in the CFD-RBD solution, the manner in which the spark range data were reduced, and inaccurate estimation because of insufficiently rich data.

Table 2. Comparison of estimated aerodynamic coefficients and estimated coefficients at Mach 3.0.

	Spark Range Data – Spark Range Reduction	**CFD-RBD – PACE**	**Percent Difference Between Coefficients**
Zero Yaw Axial Force Coefficient, C_{X0}	0.221	0.238	7.1 to 7.7
Yaw Axial Force Coefficient, C_{X2}	5.0	5.9	15.0 to 18.0
Normal Force Coefficient Derivative, C_{NA}	5.83	5.64	3.2 to 3.3
Pitching Moment Coefficient Derivative, C_{MA}	-12.6	-13.82	8.8 to 9.7
Pitch-Damping Moment Coefficient, C_{MQ}	-196	-134	31.6 to 46.3
Roll-Damping Moment Coefficient, C_{LP}	-2.71	-3.37	19.6 to 24.4

CFD-RBD data were generated at six different Mach numbers ranging from 1.5 to 4.0. The estimation algorithm discussed was used to compute a complete set of aerodynamic coefficients across its Mach range. These results are provided in table 3 with plots of the individual aerody-

namic coefficients given in figures 16 through 21. With the exception of C_{X2}, the steady aerodynamic coefficients are smooth and follow typical trends for variation in Mach number. The yaw drag coefficient, C_{X2}, however, is somewhat erratic with a low value of 0.21 at Mach 1.5 followed by a steady rise until Mach 3.5. Pitch damping decreases with Mach number, as would be expected for a fin-stabilized projectile beyond Mach 1.0. However, roll damping steadily increases until Mach 4.0 when in drops off notably.

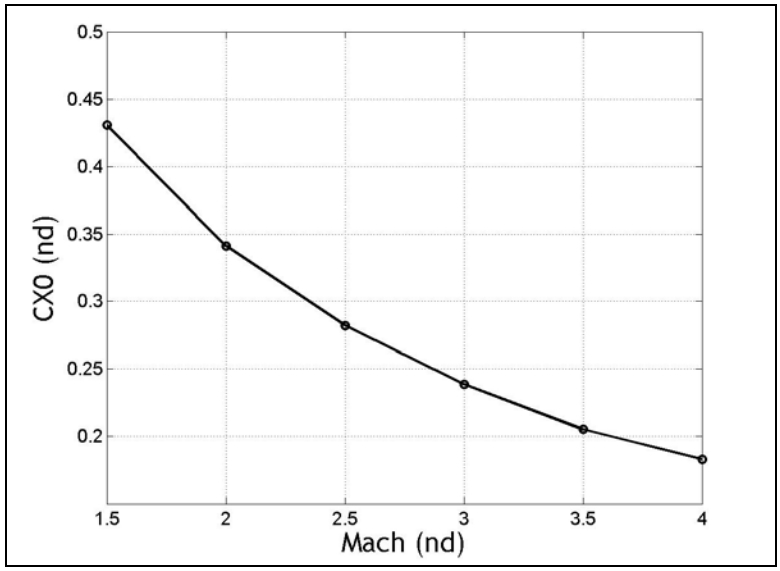

Figure 16. Zero yaw axial force coefficient versus Mach number.

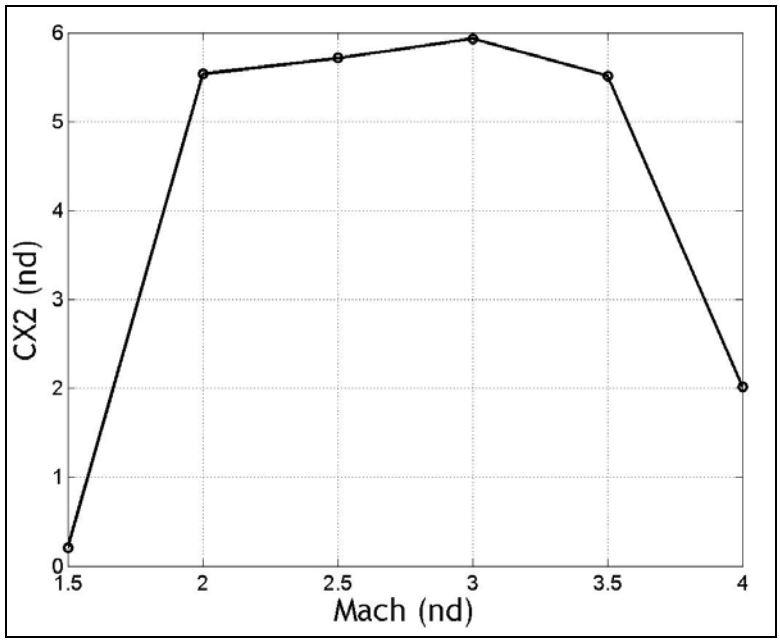

Figure 17. Yaw axial force coefficient versus Mach number.

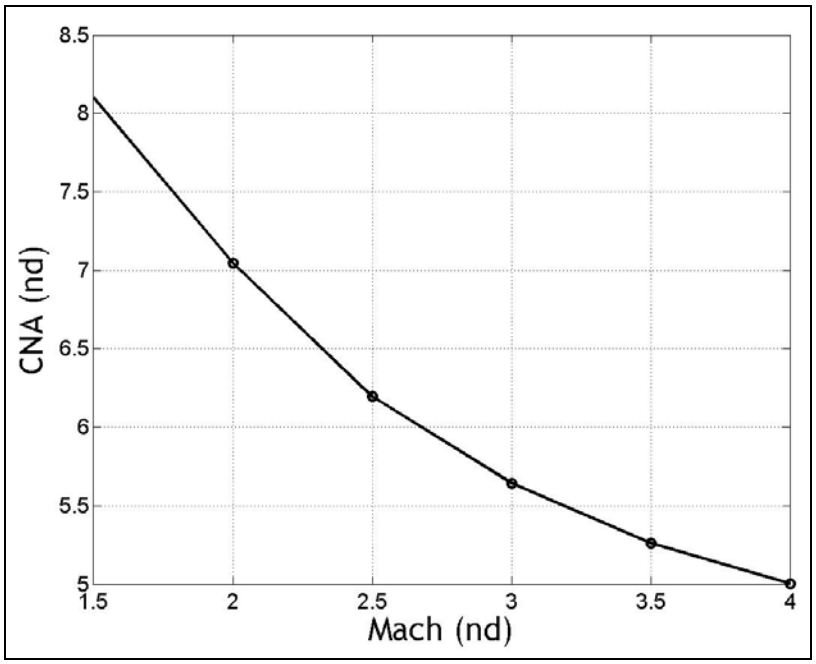

Figure 18. Normal force coefficient versus Mach number.

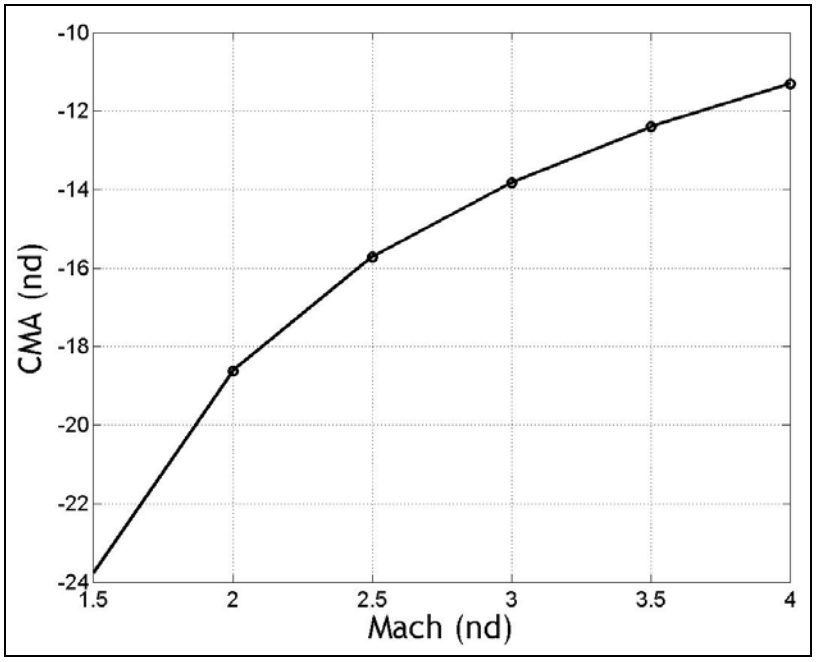

Figure 19. Pitching moment coefficient versus Mach number.

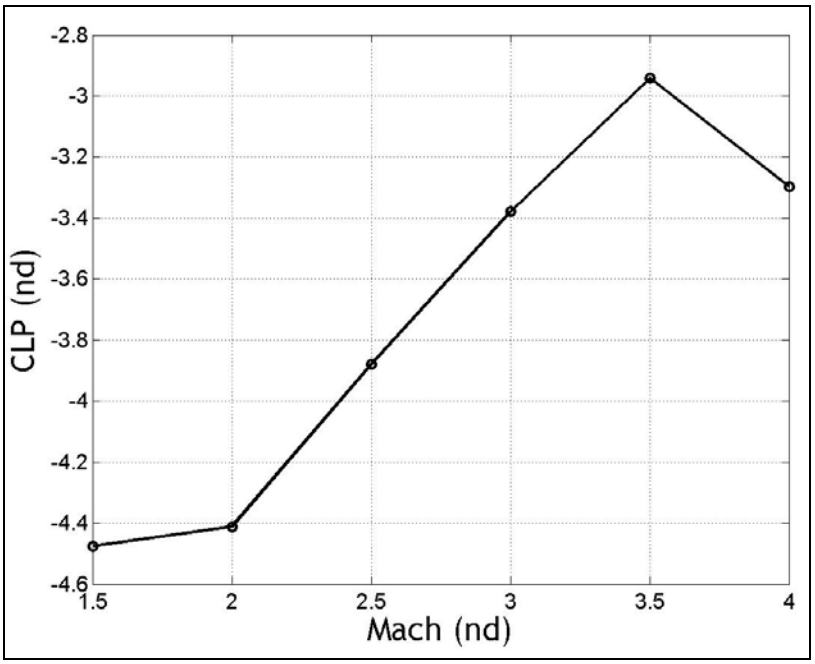

Figure 20. Roll damping moment coefficient versus Mach number.

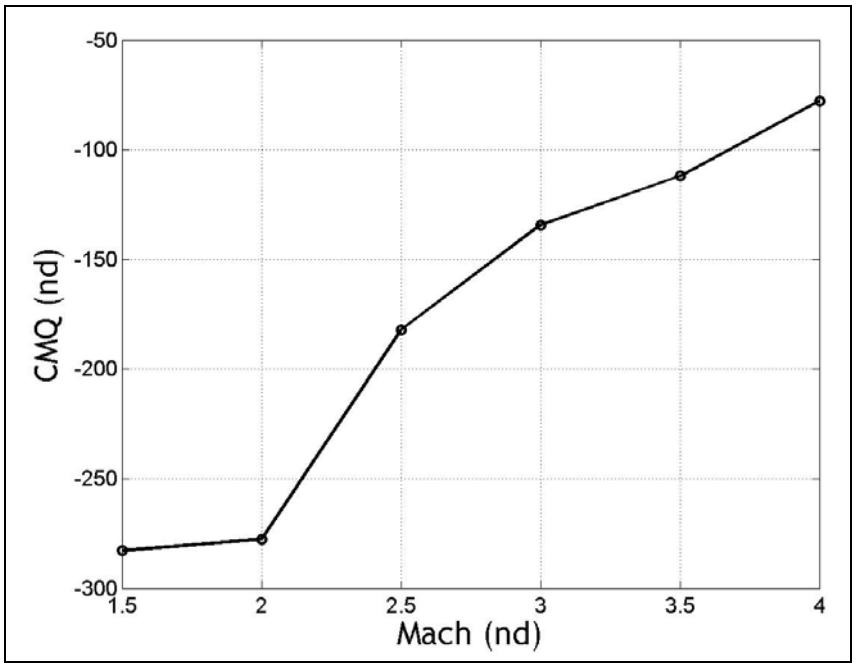

Figure 21. Pitch-damping moment coefficient versus Mach number.

In order to investigate convergence of the estimation procedure, the number of points used per time snippet was varied from a single point per time snippet to 50 points per time snippet. Of all the coefficients, the pitch-damping coefficient generally required the most number of points to converge. Figure 22 plots estimated pitch-damping coefficient versus the number of points per time snippet. For this aerodynamic coefficient, convergence is reached after about 50 points per time snippet. The points extracted from each time snippet are from the beginning of the time history and are not evenly extracted over the entire time history.

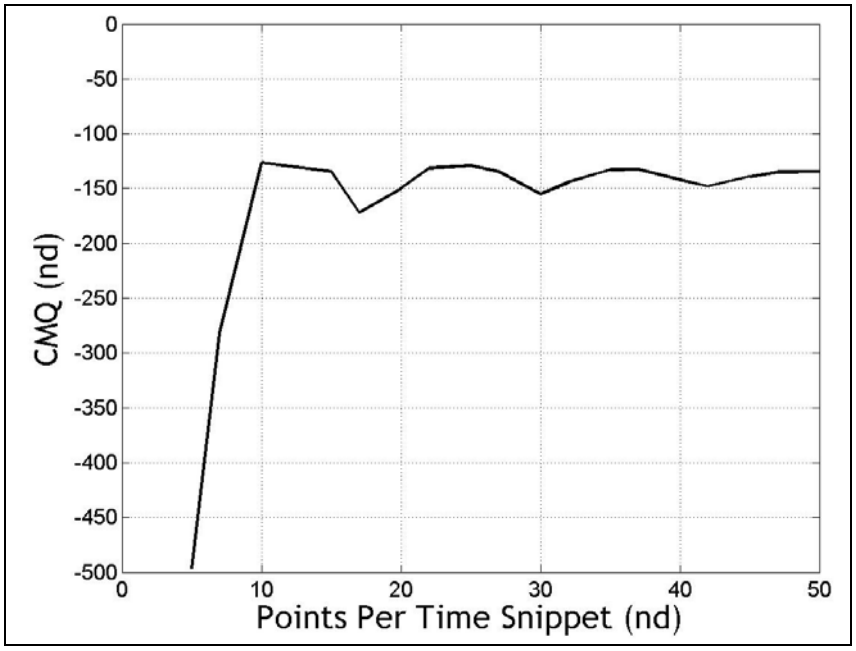

Figure 22. Pitch-damping moment coefficient versus number of points per time snippet.

6. Conclusions

With a time-accurate CFD simulation that is tightly coupled to an RBD simulation, a method to efficiently generate a complete aerodynamic description for projectile flight dynamic modeling is described. A set of n short time snippets of simulated projectile motion at m different Mach numbers is computed and employed as baseline data. The combined CFD-RBD analysis computes time-synchronized air loads and projectile state vector information, leading to a straightforward fitting procedure to obtain the aerodynamic coefficients. The estimation procedure decouples into five sub-problems that are each solved via linear least squares. The method has been applied to a sample supersonic finned projectile. Overall, the results are encouraging. A comparison of spark range obtained aerodynamic coefficients with the estimation method presented here at Mach 3 exhibits good agreement within 10% for C_{X0}, C_{NA}, and C_{MA}; agreement within 20% for C_{X2} and C_{LP}; and poor agreement within 40% for C_{MQ}. Convergence of the aerodynamic coefficients is a

strong function of the number of points in each time snippet with pitch damping generally requiring the most number of points for convergence. This technique reported here provides a promising new means for the CFD analyst to predict aerodynamic coefficients for flight dynamic simulation purposes. It can easily be extended to flight dynamic modeling of different control effectors, provided that accurate CFD-RBD time simulation is possible and an aerodynamic coefficient expansion is defined which includes the effect of the control mechanism.

7. References

1. Sun, J.; Cummings, R. Evaluation of Missile Aerodynamic Characteristics Using Rapid Prediction Techniques. *Journal of Spacecraft and Rockets* **1984**, *21* (*6*), 513-520.

2. Moore, F. The 2005 Version of the Aeroprediction Code (AP05). AIAA 2004-4715, *AIAA Atmospheric Flight Mechanics Conference*, Providence, Rhode Island, 2004.

3. Sooy, T.; Schmidt, R. Aerodynamic Predictions, Comparisons, and Validations Using Missile DATCOM and Aeroprediction 98. AIAA-2004-1246, *AIAA Aerospace Sciences Meeting and Exhibit*, Reno, Nevada, 2004.

4. Simon, J.; Blake, W. Missile DATCOM – High Angle of Attack Capabilities. AIAA-1999-4258, *AIAA Atmospheric Flight Mechanics Conference*, Portland, Oregon, 1999.

5. Neely, A.; Auman, I. Missile DATCOM Transonic Drag Improvements for Hemispherical Nose Shapes. AIAA-2003-3668, *AIAA Applied Aerodynamics Conference*, 2003.

6. Blake, W. Missile DATCOM – 1997 Status and Future Plans. AIAA-1997-2280, *AIAA Applied Aerodynamics Conference*, Atlanta, Georgia, 1997.

7. Dupuis, A.; Berner, C. Wind Tunnel Tests of a Long Range Artillery Shell Concept. AIAA-2002-4416, *AIAA Atmospheric Flight Mechanics Conference*, Monterey, California, 2002.

8. Berner, C.; Dupuis, A. Wind Tunnel Tests of a Grid Fin Projectile Configuration. AIAA-2001-0105, *AIAA Aerospace Sciences Meeting*, Reno, Nevada, 2001.

9. Evans, J. Prediction of Tubular Projectile Aerodynamics Using the ZUES Euler Code. *Journal of Spacecraft and Rockets* **1989**, *26* (5), 314-321.

10. Sturek, W.; Nietubicz, C.; Sahu, J.; Weinacht, P. Applications of Computational Fluid Dynamics to the Aerodynamics of Army Projectiles. *Journal of Spacecraft and Rockets* **1994**, *31* (2), 186-199.

11. Nusca, M.; Chakravarthy, S.; Goldberg, U. Computational Fluid Dynamics Capability for the Solid-Fuel Ramjet Projectile. *Journal of Propulsion and Power* **1990**, *6* (3).

12. Silton, S. Navier-Stokes Computations for a Spinning Projectile from Subsonic to Supersonic Speeds. *Journal of Spacecraft and Rockets* **2005**, *42* (2), 223-231.

13. DeSpirito, J.; Vaughn, M.; Washington, D. Numerical Investigation of Canard-Controlled Missile with Planar Grid Fins. *Journal of Spacecraft and Rockets* **2003**, *40* (3), 363-370.

14. Sahu, J. Numerical Computations of Transonic Critical Aerodynamic Behavior. *AIAA Journal* **May 1990**, *28* (5), 807-816.

15. Weinacht, P. Navier-Stokes Prediction of the Individual Components of the Pitch Damping Sum. *Journal of Spacecraft and Rockets* **1998**, *35* (5), 598-605.

16. Guidos, B.; Weinacht, P.; Dolling, D. Navier-Stokes Computations for Pointed, Spherical, and Flat Tipped Shells at Mach 3. *Journal of Spacecraft and Rockets* **1992**, *29* (3), 305-311.

17. Sahu, J.; Nietubicz, C. J. Application of Chimera Technique to Projectiles in Relative Motion. *Journal of Spacecraft & Rockets* **Sept-Oct 1995**.

18. Park, S.; Kwon, J. Navier-Stokes Computations of Stability Derivatives for symmetric Projectiles. AIAA-2004-0014, *AIAA Aerospace Sciences Meeting*, Reno, Nevada, 2004.

19. Sahu, J. Numerical Simulations of Supersonic Flow over an Elliptic-Section Projectile with Jet-Interaction. *AIAA Paper No. 2002-3260*, St. Louis, MO, 24-27 June 2002.

20. Qin, N.; Ludlow, K.; Shaw, S.; Edwards, J.; Dupuis, A. Calculation of Pitch Damping for a Flared Projectile. *Journal of Spacecraft and Rockets* **1997**, *34* (4), 566-568.

21. Weinacht, P. Coupled CFD/GN&C Modeling for a Smart Material Canard Actuator. AIAA-2004-4712, *AIAA Atmospheric Flight Mechanics Conference*, Providence, Rhode Island, 2004.

22. Park, S.; Kim, Y.; Kwon, J. Prediction of Dynamic Damping Coefficients Using Unsteady Dual Time Stepping Method. AIAA-2002-0715, *AIAA Aerospace Sciences Meeting*, Reno, Nevada, 2002.

23. DeSpirito, J.; Heavey, K. CFD Computation of Magnus Moment and Roll-Damping Moment of a Spinning Projectile. AIAA-2004-4713, *AIAA Atmospheric Flight Mechanics Conference*, Providence, Rhode Island, 2004.

24. Sahu, J.; Heavey, K. R. Unsteady CFD Modeling of Micro-Adaptive Flow Control for an Axisymmetric Body. *International Journal of Computational Fluid Dynamics* **April-May 2006**, *5*.

25. Garon, K.; Abate, G.; Hathaway, W. Free-Flight Testing of a Generic Missile with MEMs Protuberances. AIAA -2003-1242, *AIAA Aerospace Sciences Meeting*, Reno, Nevada, 2003.

26. Kruggel, B. High Angle of Attack Free Flight Missile Testing. AIAA-1999-0435, *AIAA Aerospace Sciences Meeting*, Reno, Nevada, 1999.

27. Danberg, J.; Sigal, A.; Clemins, I. Aerodynamic Characteristics of a Family of Cone-Cylinder-Flare Projectiles. *Journal of Spacecraft and Rockets* **1990**, *27* (4).

28. Dupuis, A. Free-Flight Aerodynamic Characteristics of a Practice Bomb at Subsonic and Transonic Velocities. AIAA-2002-4414, *AIAA Atmospheric Flight Mechanics Conference*, Monterey, California, 2002.

29. Abate, G.; Duckerschein, R.; Hathaway, W. Subsonic/transonic Free-Flight Tests of a Generic Missile with Grid Fins. AIAA-2000-0937, *AIAA Aerospace Sciences Meeting*, Reno, Nevada, 2000.

30. Chapman, G.; Kirk, D. A Method for Extracting Aerodynamic Coefficients from Free-Flight Data. *AIAA Journal* **1970**, *8* (4), 753-758.

31. Abate, G.; Klomfass, A. Affect upon Aeroballistic Parameter Identification from Flight Data Errors. *AIAA Aerospace Sciences Meeting*, Reno, Nevada, 2005.

32. Abate, G.; Klomfass, A. A New Method for Obtaining Aeroballistic Parameters from Flight Data. *Aeroballistic Range Association Meeting*, Freiburg, Germany, 2004.

33. Weinacht, P.; Sturek, W.; Schiff, L. Projectile Performance, Stability, and Free-Flight Motion Prediction Using Computational Fluid Dynamics. *Journal of Spacecraft and Rockets* **2004**, 41 (2), 257-263.

34. Sahu, J. Time-Accurate Numerical Prediction of Free-Flight Aerodynamics of a Finned Projectile. AIAA-2005-5817, *AIAA Atmospheric Flight Mechanics Conference*, San Francisco, California, 2005.

35. Peroomian, O.; Chakravarthy, S.; Goldberg, U. A 'Grid-Transparent' Methodology for CFD. *AIAA Paper 97-07245*, 1997.

36. Peroomian, O.; Chakravarthy, S.; Palaniswamy, S.; Goldberg, U. Convergence Acceleration for Unified-Grid Formulation Using Preconditioned Implicit Relaxation. *AIAA Paper 98-0116*, 1998.

37. Abate, G.; Klomfass, A. Affect upon Aeroballistic Parameter Identification from Flight Data Errors. AIAA-2005-0439, *AIAA Aerospace Sciences Meeting*, Reno, Nevada, 2005.

NO. OF COPIES ORGANIZATION

1 (PDF ONLY) DEFENSE TECHNICAL INFORMATION CTR DTIC OCA
8725 JOHN J KINGMAN RD
STE 0944
FORT BELVOIR VA 22060-6218

1 US ARMY RSRCH DEV & ENGRG CMD
SYSTEMS OF SYSTEMS INTEGRATION
AMSRD SS T
6000 6TH ST STE 100
FORT BELVOIR VA 22060-5608

1 DIRECTOR
US ARMY RESEARCH LAB
IMNE ALC IMS
2800 POWDER MILL RD
ADELPHI MD 20783-1197

1 DIRECTOR
US ARMY RESEARCH LAB
AMSRD ARL CI OK TL
2800 POWDER MILL RD
ADELPHI MD 20783-1197

2 DIRECTOR
US ARMY RESEARCH LAB
AMSRD ARL CI OK T
2800 POWDER MILL RD
ADELPHI MD 20783-1197

1 AEROPREDICTION INC
F MOORE
9449 GROVER DRIVE, STE 201
KING GEORGE VA 22485

1 UNIV OF TEXAS AT ARLINGTON
MECH & AEROSPACE ENGINEERING DEPT
ATTN J C DUTTON
BOX 19018
500 W FIRST ST
ARLINGTON TX 76019-0018

2 ATK TACTICAL SYSTEMS DIV
ALLEGANY BALLISTICS LAB
ATTN D J LEWIS J S OWENS
210 STATE ROUTE 956
ROCKET CENTER WV 26726

1 ATK ADVANCED WEAPONS DIV
ATTN R H DOHRN
MN06-1000
4600 NATHAN LANE N
PLYMOUTH MN 55442

NO. OF COPIES ORGANIZATION

1 ATK ORDNANCE SYS
ATTN B BECKER
MN07 MW44
4700 NATHAN LANE N
PLYMOUTH MN 55442

1 SCIENCE APPLICATIONS INTL CORP
ATTN J NORTHRUP
8500 NORMANDALE LAKE BLVD
SUITE 1610
BLOOMINGTON MN 55437

3 GOODRICH ACTUATION SYSTEMS
ATTN T KELLY P FRANZ
J CHRISTIANA
100 PANTON ROAD
VERGENNES VT 05491

2 ARROW TECH ASSOC
ATTN W HATHAWAY J WHYTE
1233 SHELBURNE RD STE D8
SOUTH BURLINGTON VT 05403

1 KLINE ENGINEERING CO INC
ATTN R W KLINE
27 FREDON GREENDEL RD
NEWTON NJ 07860-5213

1 GEORGIA INST TECH
DEPT AEROSPACE ENGR
ATTN M COSTELLO
270 FERST STREET
ATLANTA GA 30332

1 AIR FORCE RSRCH LAB
AFRL/MNAV
ATTN G ABATE
101 W EGLIN BLVD STE 333
EGLIN AFB FL 32542-6810

1 US ARMY RDECOM ARDEC
ATTN AMSRD AAR AEM A G MALEJKO
BLDG 95
PICATINNY ARSENAL NJ 07806-5000

2 US ARMY ARDEC
ATTN AMSRD AAR AEP E D CARLUCCI
ATTN AMSRD AAR AEP E I MEHMEDAGIC
BLDG 94
PICATINNY ARSENAL NJ 07806-5000

1 US ARMY TACOM ARDEC
ATTN AMSRD AAR AEP E C KESSLER
BLDG 3022
PICATINNY ARSENAL NJ 07806-5000

NO. OF
COPIES ORGANIZATION

1 APM SMALL & MED CALIBER AMMO
OPM MAS
ATTN SFAE AMO MAS SMC
R KOWALSKI
BLDG 354
PICATINNY ARSENAL NJ 07806-5000

3 US ARMY AMRDEC
ATTN AMSAM RD SS AT L AUMAN
R W KRETZSHMAR
E VAUGHN
REDSTONE ARSENAL AL 35898-5000

ABERDEEN PROVING GROUND

1 DIRECTOR
US ARMY RSCH LABORATORY
ATTN AMSRD ARL CI OK (TECH LIB)
BLDG 4600

18 DIR USARL
AMSRD WM
J SMITH
AMSRD WM B
M ZOLTOSKI
AMSRD WM BA
D LYON
AMSRD WM BC
P PLOSTINS
I CELMINS
M CHEN
J DESPIRITO
B GUIDOS
K HEAVEY
J SAHU
S SILTON
P WEINACHT
F FRESCONI
M BUNDY
G COOPER
B HOWELL
AMSRD WM BD
B FORCH
AMSRD WM BF
J NEWILL
S WILKERSON
H EDGE

FOREIGN ADDRESSES

1 DSTL BEDFORD
T BIRCH
BLDG 115 RM 125
BEDFORD TECHNOLOGY PARK
BEDFORD
MK44 2FQ
UK

2 DEFENCE RESEARCH AND
DEVELOPMENT CANADA
VALCARTIER
F LESAGE
E FOURNIER
2459 PIE-XI BLVD NORTH
VAL BELAIR QC G3J1X5
CANADA